Eco-Friendly Synthesis of Zinc Oxide Using Green Alkaline Solution for Enhanced Solar-Driven Photocatalytic Degradation of Methylene Blue

Nedra Abbes[1,2], Sana Fridjine[3], Thouraya Barhoumi[3], Nejib Sejri[2], Boubaker Jaouachi[4], Jun Xu[1*], and Imene Bekri-Abbes[5]

[1]*School of Textile Science and Engineering, Tiangong University, Tianjin 300000, China*

[2]*Textile Engineering Laboratory (LGTEX), Higher Institute of Technical Studies of Ksar Hellal (ISET), University of Monastir, Monastir 5000, Tunisia*

[3]*Physical Chemistry Laboratory for Mineral Materials and Their Applications, National Center for Research in Materials Sciences, Borj Cedria Technopark, Soliman 8027, Tunisia*

[4]*National School of Engineers of Monastir, University of Monastir, Monastir 5000, Tunisia*

[5]*Laboratory of Composite Materials and Clay Minerals, National Center of Materials Research, Borj Cedria Technopark, Slimene 2084, Tunisia*

* ***Corresponding author:***

tel: +86-18920911580
email: xujun@tiangong.edu.cn

Received: October 12, 2025
Accepted: December 8, 2025

DOI: 10.22146/ijc.112000

Abstract: *Zinc oxide (ZnO) particles were green-synthesized using an aqueous extract of olive wood ash as a sustainable alkaline precipitating agent. The extract pH stabilized near 13 (40 wt.%), confirming strong alkalinity. A two-step process involved forming a zinc carbonate precursor, followed by calcination at 900 °C. X-ray diffraction confirmed highly crystalline hexagonal wurtzite ZnO. Optical analysis revealed a reduced bandgap of 2.80 eV, significantly lower than the conventional value of 3.37 eV, attributed to lattice defects and elemental incorporation. Evaluating the photocatalytic efficiency against methylene blue under natural solar light, the green-synthesized ZnO achieved nearly 99% removal within 2 h, outperforming conventional ZnO due to enhanced solar absorption from its narrowed bandgap. This work validates a zero-waste pathway for synthesizing highly active nanomaterials, setting a strong precedent for circular economy applications in sustainable photocatalysis.*

Keywords: *bandgap; methylene blue; olive wood ash; photocatalysis; zinc oxide*

■ INTRODUCTION

The growing demand for advanced materials across diverse technological sectors has led to significant focus on the synthesis of nanoparticles. Among these, zinc oxide (ZnO) nanoparticles are particularly prominent due to their unique physicochemical properties, including a wide direct bandgap with 3.37 eV, high exciton binding energy with 60 meV, and excellent optical, electrical, and catalytic characteristics [1]. Traditionally, ZnO nanoparticles are synthesized using various conventional methods, such as wet chemical routes [2] and precipitation techniques [3-4]. While these methods offer control over size and morphology, they frequently rely on expensive instrumentation, consume high energy, and, critically, necessitate the use of toxic and hazardous chemical reagents. These limitations pose significant environmental concerns, contribute to high production costs, and highlight an urgent global imperative for simpler, more eco-friendly, and economically viable alternatives. In response to these challenges, the field of green synthesis has emerged as a promising and sustainable paradigm for nanoparticle production [5-6]. This approach leverages natural, benign sources (such as plant and microbial extracts), which contain biomolecules that act as effective reducing and/or capping agents, facilitating nanoparticle formation in an environmentally benign manner [7-9].

Building upon the principles of sustainable chemistry and waste valorization, this study focuses on olive wood charcoal ash (OWCA) as a novel and highly promising precursor for ZnO nanoparticle synthesis [10]. OWCA is a readily available and sustainable by-product generated from the combustion of olive wood, a common practice in many rural communities. Chemical analysis reveals that OWCA is rich in various alkaline compounds, predominantly calcite ($CaCO_3$) and calcium oxide (CaO), along with significant trace minerals such as potassium, magnesium, and phosphorus. These inherent components not only make OWCA a valuable resource in agriculture for soil enhancement and pest control [11] but also, crucially, impart a high alkalinity to its aqueous extracts. More pertinently, due to the substantial presence of alkaline compounds like potassium carbonate (K_2CO_3) and potassium hydroxide (KOH), ash water has been successfully employed in various green synthesis methods for producing a diverse array of compounds, including other forms of zinc oxide catalysts. Building upon this established sustainable approach, the primary objective of the present study is to synthesize zinc oxide nanoparticles using an aqueous OWCA extract as a sustainable, cost-effective, and eco-friendly alkali source.

The continuous contamination of water streams by industrial pollutants, including recalcitrant organic dyes, represents one of the most pressing global environmental challenges. To address this, photocatalysis using semiconductor metal oxides is a highly promising and sustainable method [12-13]. ZnO is particularly valued as a photocatalyst for its superior photosensitivity, high catalytic activity, suitable bandgap, low cost, and overall eco-friendliness [14]. In the textile industry, methylene blue (MB) is extensively applied in the production of copy paper, printing inks, and in the dyeing of fabrics such as cotton, silk, wool, and leather, where it also serves as a mordant. Due to its complex molecular structure, MB exhibits strong resistance to conventional chemical, physical, and biological treatment methods. Exposure to MB has been associated with several adverse health effects, including methemoglobinemia, vomiting, respiratory distress, mental disorientation, and ocular irritation [15]. For this reason, MB was selected as a model pollutant to evaluate the photocatalytic efficiency (PE) of the synthesized catalysts.

Although ZnO has indeed been synthesized by numerous green and chemical routes in the literature, the present work introduces a novel and previously unreported approach: this is the first study to successfully utilize an aqueous extract of OWCA as a completely natural, waste-derived alkaline precipitating agent for the synthesis of ZnO. This innovative approach aims to not only provide a greener synthesis route but also to investigate the impact of this sustainable method on the structural, optical, and, most importantly, the photocatalytic properties of the resulting ZnO nanoparticles, particularly their efficiency in environmental remediation under natural solar light. This innovative approach is uniquely aligned with circular economy principles, as it valorizes a waste stream into a high-value material. The primary objective of the present study is to synthesize zinc oxide nanoparticles ZnO using an aqueous OWCA extract as a sustainable, cost-effective, and eco-friendly alkali source. This study investigates the impact of this sustainable method on the structural, optical, and, most importantly, the photocatalytic properties of the resulting ZnO nanoparticles, demonstrating their efficiency in environmental remediation under natural solar light.

■ EXPERIMENTAL SECTION

Materials

All chemicals, including zinc acetate dihydrate (99.99%), and sodium hydroxide (98%), and MB were sourced from Aldrich and used as received. Distilled water was used throughout all experiments.

Instrumentation

X-ray diffraction (XRD) spectra were obtained using an X'Pert Pro PANalytical X-ray diffractometer and a D8 ADVANCE system from Bruker, United States of America (USA). The diffractograms were processed with X'Pert High Score Plus software and was performed with a resolution of 0.02° and 30 scans. The functional groups of samples were identified using attenuated total

reflection Fourier transform infrared (ATR-FTIR) spectroscopy technique within the range of 400–4000 cm^{-1}. The analysis was conducted with a Perkin Elmer Spectrum instrument, a two-beam IR spectrophotometer equipped with an attenuated total reflection accessory. Photoluminescence (PL) spectra were recorded using Fluorolog–FL3-11 fluorescence spectrometer. Scanning electron microscopy (SEM) images of the selected samples were captured using a Quanta 650 scanning electron microscope, with a resolution range from 30× to 200,000×, and an accelerating voltage varying between 0.2 and 30 kV. The pH of the solution was monitored with a calibrated digital pH meter (S-610H).

Procedure

Preparation of OWCA water extract and characterization

OWCA is commonly used in rural Tunisian families for cooking. The ash of this charcoal was collected for this study and was mixed with distilled water at varying concentrations of 10, 20, and 40% w/v to prepare the ash water extract. Each mixture was stirred continuously for 100 min at room temperature (20), 40 and 70 °C to facilitate the dissolution of soluble minerals. The solutions were filtered by centrifugation at 3500 rpm for 5 min, followed by filtration through (Whatman No. 1) filter paper to remove impurities. The pH of the solution was maintained at approximately 13. The extracts were stored in sealed containers at room temperature for further use.

Synthesis of ZnO

ZnO was synthesized via a precipitation method using zinc acetate dihydrate and water extracts of olive wood ash. In a typical procedure, 0.1 g of zinc acetate dihydrate was dissolved in 200 mL of olive wood ash water extract (prepared at a concentration of 10% w/v. Immediately after the addition of zinc acetate solution, the reaction started and the solution became white and cloudy. The reaction continued for 2 h and then the suspension produced was kept still overnight to precipitate. After the reaction, the resultant precipitate was allowed to settle for 48 h at room temperature. The precipitate was then separated from the reaction solution by centrifugation at 4,000 rpm for 10 min and repeatedly washed with deionized water to remove any soluble impurities. Finally, the purified product was dried in an oven at 80 °C for 24 h and heated at 900 °C for 2 h in a muffle furnace to yield ZnO as a fine powder. For comparison, ZnO has been prepared by the conventional precipitation method using NaOH as an alkaline solution. A 0.1 M zinc acetate dihydrate solution and a 0.2 M NaOH solution were prepared in double-distilled water. The zinc acetate solution was heated to 80 °C while stirring, and the NaOH solution was added slowly, resulting in the formation of a zinc hydroxide precipitate. After stirring for 1 h, the mixture was cooled, and the precipitate was purified by repeated washing with distilled water. The purified precipitate was then dried in an oven. Finally, the dried zinc hydroxide powder was transferred to a furnace and calcined at 450 °C for 2 h to convert it into stable ZnO powder.

Experimental protocol for solar-driven MB photodegradation

The photocatalytic performance of the synthesized ZnO nanoparticles was evaluated through the degradation of MB dye under natural solar irradiation. Experiments were conducted outdoors in Borj Cedria, Ben Arous Governorate, Tunisia (36°43'04"N, 10°25'41"E), on July 22, 2025, under clear daylight conditions to maximize solar exposure. The site is characterized by strong summer irradiation. On the test day, a clear summer day, experiments were carried out between 12:00 PM and 3:00 PM local time (CET), corresponding to the period of maximum solar intensity. Sunrise occurred at approximately 5:00 AM and sunset at 7:40 PM, providing about 14.5 h of daylight. In July, Borj Cedria typically records an average global horizontal irradiance (GHI) of 4.2–5.0 kWh/m^2/day, with midday peak values under clear skies ranging from 800 to 1000 W/m^2. A stock solution of MB with 1 g/L was first prepared by dissolving the required amount of dye in distilled water, then 25 mg/L solution was prepared by dilution. An amount of 50 mL of the solution was transferred to a clean beaker, and 50 mg of ZnO nanoparticles was accurately dispersed

into it. The suspensions were initially stirred in the dark for 24 h to establish adsorption–desorption equilibrium between the dye molecules and the ZnO surface, ensuring that subsequent color reduction could be attributed to photocatalysis rather than mere adsorption. After equilibrium, the beakers were exposed to direct solar light under static condition without stirring and aliquots were withdrawn during irradiation. Each sample was immediately centrifuged to separate the photocatalyst, and the supernatant was analyzed using UV–vis spectrophotometry at the $\lambda = 400–800$ nm ($\lambda_{max} \approx 660$ nm). The degradation efficiency (%) was calculated using Eq.(1) [16];

$$\text{Degradation efficiency} = \frac{C_0 - C_t}{C_0} \times 100 \quad (1)$$

where, C_0 is the initial dye concentration after the adsorption step, and C_t is the concentration at irradiation time t. After completion of the photocatalytic degradation experiments, the green-synthesized ZnO nanoparticles were easily and quantitatively recovered from the treated MB solution by simple filtration through a Whatman® Grade 42 quantitative filter paper (pore size 2.5 or 11 μm) followed by rinsing with distilled water.

■ RESULTS AND DISCUSSION

Characterization of ZnO

XRD

The precipitate obtained from the reaction of OWCA extract and zinc acetate was collected and thoroughly characterized using powder XRD. The resulting diffraction pattern, as shown in Fig. 1(a) confirms the successful formation of highly crystalline ZnO synthesized using the olive wood ash extract with a hexagonal wurtzite structure. This rigorous structure is essential not merely for physical stability, but for controlling the electronic fate of photogenerated charge carriers. The successful synthesis of crystalline ZnO was confirmed by XRD analysis, which showed characteristic reflection peaks at (100), (002), (101), (102), (103), (110), and (004), all consistent with the hexagonal wurtzite structure of ZnO [17-18]. In addition, these findings align with previous study [19]. The most intense peak at 36.2°, assigned to the (101) crystallographic plane, further evidences typical ZnO growth [17]. This finding suggests that the precursor was not completely converted during calcination, highlighting a potential area for optimizing the calcination temperature and/or duration to enhance final product purity. The crystallite size of the green-synthesized ZnO was calculated from the XRD pattern shown in Fig. 1(a) using Eq. (2);

$$D = \frac{K\lambda}{\beta}\cos\theta \quad (2)$$

where D represents the crystallite size (nm), K = 0.89 is the shape factor, λ is the wavelength of the Cu Kα radiation, and β is the corrected full width at half maximum (FWHM) of the diffraction peak. The diffraction angle 2θ = 36.2°, corresponding to the (101) plane of ZnO, was used to calculate the crystallite size, which was found to be 37 nm.

FTIR

The successful formation of zinc oxide was further confirmed by the FTIR spectrum, as illustrated in Fig. 1(b). The spectrum revealed characteristic absorption peaks at 3508, 3402, 1553, 1389, 1340, 1021, 833, 677, 518, and 475 cm^{-1}. The broad bands observed at 3508 and 3402 cm^{-1} are attributed to O–H stretching vibrations, indicating the presence of adsorbed water molecules and/or surface hydroxyl groups on the material [20]. The presence of these hydroxyl groups is beneficial for photocatalysis as they serve as active sites for the generation of hydroxyl radicals (OH). The band at 1021 cm^{-1} corresponds C–O stretching vibrations, likely originating from minor residual organic components from the ash extract [21]. Crucially, the spectrum also shows strong absorption bands corresponding to carbonate (CO_3^{2-}) vibrational modes, including a peak at 1553 cm^{-1} assigned to the asymmetric stretching (ν3) of a carbonate or bicarbonate species. The prominent peak at 1389 cm^{-1} is characteristic of the asymmetric stretching (ν3) of a free or slightly perturbed carbonate ion, consistent with residual carbonate phases like $CaCO_3$ or unreacted precursor [22]. The peak at 1340 cm^{-1} might be associated with symmetric stretching or in-plane bending of carbonates, or possibly minor C–H bending from organic residues [23]. Finally, the strong absorption bands at 518 and 475 cm^{-1} are characteristic of

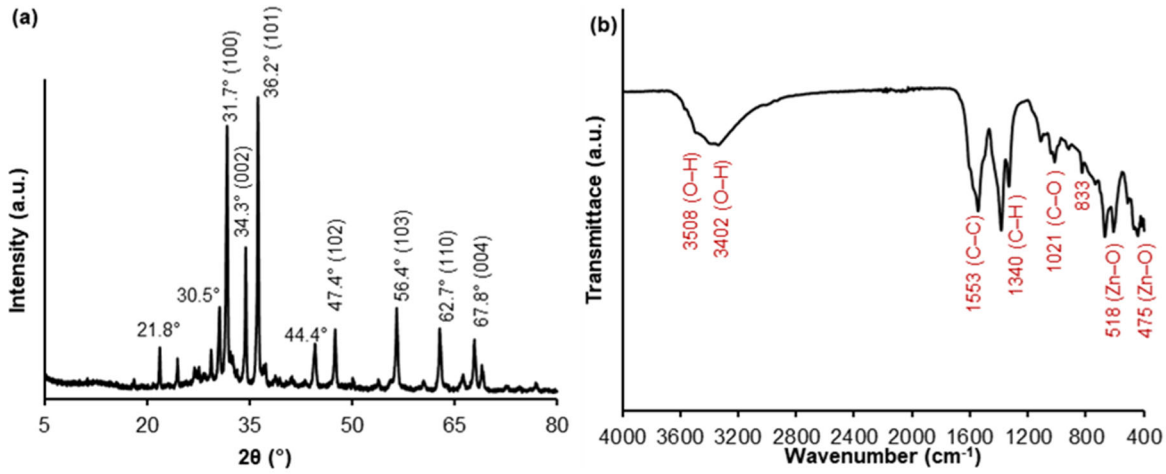

Fig 1. (a) XRD pattern and (b) FTIR spectrum of the synthesized ZnO nanoparticles

the metal-oxygen (Zn–O) stretching vibrations in the hexagonal wurtzite structure of ZnO [24]. The FTIR analysis is crucial for detecting the presence of Zn–O bonds and identifying any residual organic functional groups from the olive wood ash extract that may be incorporated into the final ZnO product. This provides evidence of the bio-mediated synthesis process, and its effect on the material's compositions.

SEM

The images of the green-synthesized ZnO nanoparticles, presented at various magnifications, provide crucial visual evidence of their morphological characteristics, particle arrangement, and surface features. At lower magnifications, the images reveal that the ZnO material predominantly exists as irregular aggregates [25]. These aggregates form a porous and interconnected network, rather than a collection of isolated, discrete nanoparticles. This observed aggregation is a common phenomenon in synthesized nanomaterials, particularly those produced via precipitation and subsequent calcination, often driven by the inherent high surface energy of nanoparticles and strong inter-particle forces [26]. As the magnification is increased, particularly in the images with 1 µm and 500 nm scale bars, the primary particles generally exhibit irregular, polyhedral, or granular shapes, deviating from perfectly spherical (Fig. 2). The observed morphology is a key factor in the photocatalytic efficiency of the synthesized ZnO nanoparticles. The irregular shape and porous, aggregated structure revealed by SEM provide a high surface area-to-volume ratio [26-27]. This is crucial for photocatalysis, as it increases the number of available active sites for the adsorption of dye molecules and the subsequent generation of reactive oxygen species. This enhanced surface-area-dependent adsorption, combined with the material's favorable light absorption properties, directly contributes to the superior degradation performance of the green-synthesized photocatalyst [28]. The porous network also allows for better light penetration and reduced particle aggregation in the solution, further boosting the overall efficiency. The difference in calcination temperature profoundly affects the structural and functional properties of the synthesized ZnO. Furthermore, SEM analysis confirms extensive agglomeration of the ZnO particles into micrometric clusters. The discernible primary crystallites display irregular shapes and a broad size distribution ranging from 120 to 950 nm.

Determination of Band Gap Using Kubelka-Munk Model

Absorption spectra of the ZnO and ZnO derived from olive wood ash powder were obtained from the diffuse reflectance value using the Kubelka-Munk function, using Eq. (3) [29];

$$F(R) = \frac{(1-R)^2}{2R} \quad (3)$$

where R is the coefficient of diffuse reflection.

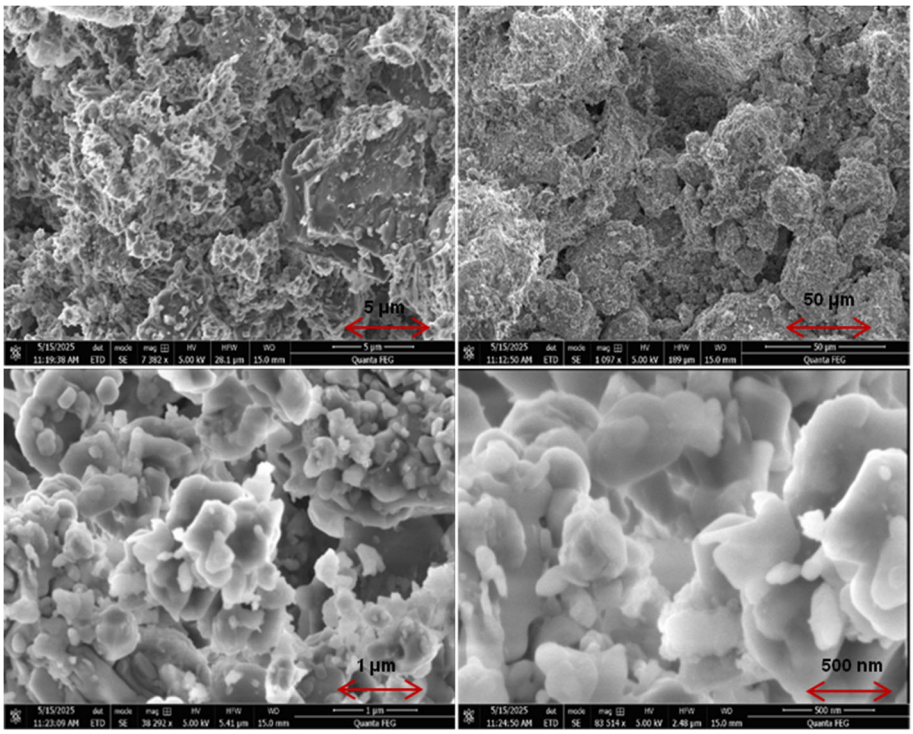

Fig 2. SEM image of green-synthesized ZnO nanoparticles at various magnifications

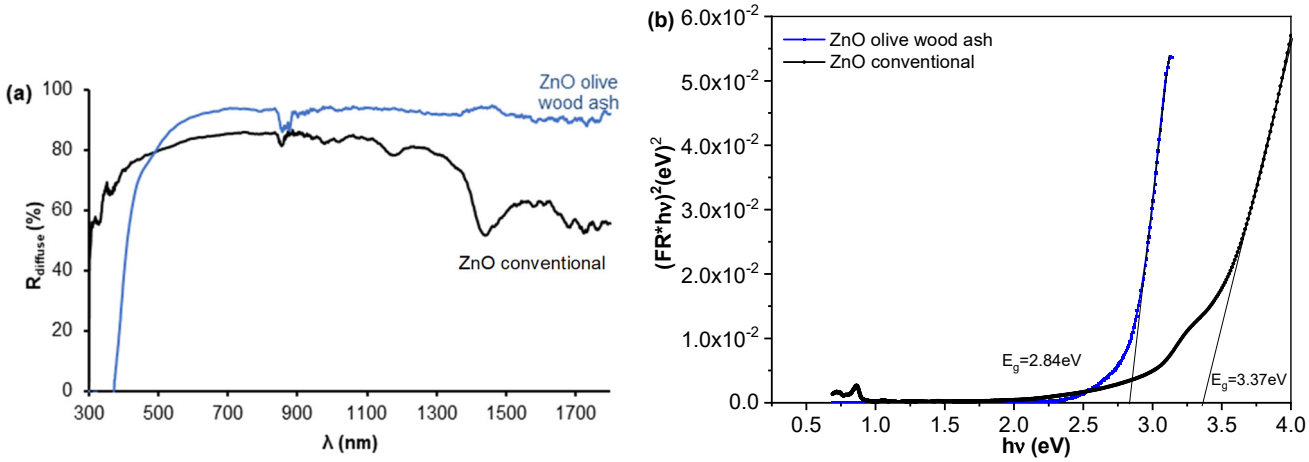

Fig 3. Optical characterization and direct band gap determination. (a) DRS spectra comparing the optical absorption of ZnO conventional (black line) and ZnO wood ash (blue line). (b) The Tauc plot is used to determine the direct optical band gap

Fig. 3(a) shows the reflectance spectroscopy spectra of ZnO synthesized from olive wood ash and the conventional ZnO. This result reveals a significant difference in their optical properties across the UV-vis-NIR spectrum. Both materials exhibit the characteristic ZnO absorption edge around 400 nm, confirming the success of green ZnO. However, ZnO obtained from olive wood ash demonstrates substantially higher reflectance values (90–95%) compared to conventional ZnO (80–85%) throughout the visible and near-infrared regions. This enhancement suggests that the bio-derived synthesis route produces ZnO with modified morphological and structural characteristics, likely including different particle sizes, surface textures, or

residual organic/mineral components from the ash precursor. The more stable reflectance profile of the ash-derived ZnO, particularly in the NIR region where conventional ZnO shows pronounced absorption features, indicates that the green synthesis approach not only provides an environmentally sustainable route to ZnO production but also yields material with potentially superior optical properties for applications requiring enhanced light scattering, such as photo-catalysis, solar cells, or optical coatings.

The optical gap value is estimated relying on the Kubelka-Munk method combined with the Tauc relation using Eq. (4) [30];

$$\left(F(R_d)h\nu\right)^2 = A\left(h\nu - E_g\right) \quad (4)$$

where hν is the photon energy, A is an energy-dependent constant. By plotting $(F(R_d)h\nu)^2$ as a function of energy excitation, it is estimated that the direct band gap of ZnO and olive wood ash ZnO is shown in Fig. 3(b).

The significant reduction in bandgap energy of the ZnO synthesized from olive wood ash (from 3.37 eV for conventional ZnO to 2.80 eV) suggests a profound modification of the electronic structure [30]. While direct compositional evidence from advanced spectroscopy is not included in this preliminary study, this bandgap narrowing is most plausibly attributed to several interconnected factors. The presence of residual organic impurities creates intermediate energy states within the bandgap, enabling lower-energy electronic transitions. Additionally, the uncontrolled synthesis conditions inherent in using natural ash sources introduce a higher concentration of structural defects such as oxygen vacancies and zinc interstitials, which form donor/acceptor levels that reduce the effective bandgap, as strongly supported by PL analysis. Finally, the ash naturally contains trace metal impurities (K, Ca, Mg, Fe) that can plausibly incorporate into the ZnO lattice structure, acting as dopants and further modifying the electronic band structure. These combined effects result in a beneficial red shift of the optical absorption edge, which is a key advantage for solar-driven photocatalytic applications.

PL Analysis

The PL spectra of synthesized ZnO, at an excitation wavelength of 350 nm, are presented in Fig. 4. In general, the spectrum reveals two distinct luminescence bands: one in the UV region and another in the visible region, each corresponding to different radiative recombination processes [31]. The result of the curve fitting showed three peaks centered at 392.5, 485.5, and 529.0 nm. The most prominent peak observed at 392.5 nm was attributed to the near band edge (NBE) emission of ZnO [32-33]. This emission originates from the radiative recombination of free excitons (electron-hole pairs) and is characteristic of the intrinsic direct bandgap of wurtzite ZnO [34-35]. The peak at 485.5 nm is observed in the blue-green region. The blue and green emissions are generally associated with Zn and the oxygen-related defects, respectively [36-37]. The presence of these defect-related visible emission bands (485.5 and 529.0 nm) is crucial for the photocatalytic performance [38]. These intrinsic defects (oxygen vacancies and zinc interstitials) function as effective trapping sites for photogenerated electrons or holes. By capturing these charge carriers, the defects significantly suppress the electron-hole recombination rate, which is often the limiting factor in semiconductor photocatalysis. This prolonged charge carrier lifetime directly contributes to a higher yield of reactive oxygen species (ROS) on the catalyst surface.

Photocatalytic Application

The beakers, containing the MB dye and the synthesized ZnO nanoparticles synthetized by green and conventional precipitation method, were exposed to

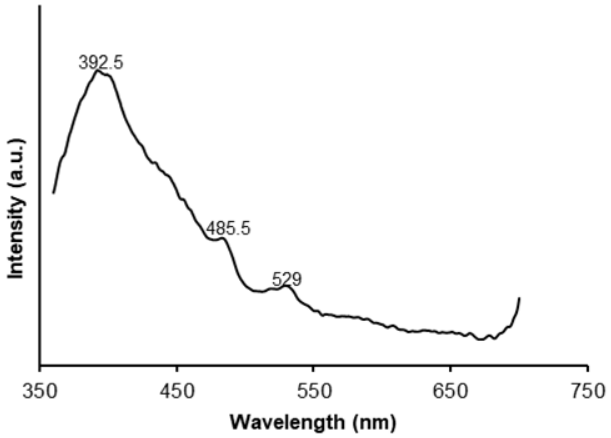

Fig 4. PL spectrum of the synthesized ZnO

natural solar irradiation outdoors at the National Center of Materials Research, Technopole of Borj Cedria, Tunisia, from 12:00 PM to 3:00 PM on July 22nd 2025. The UV–vis absorption spectra presented in Fig. 5 prove the progressive degradation of MB solution under solar light irradiation in the presence of green-synthesized ZnO nanoparticles. Initially, the MB solution at 25 mg/L exhibits a strong absorption peak centered around 664 nm, characteristic of the monomeric form of MB, accompanied by a minor shoulder peak near 610 nm. The spectrum, recorded after 24 h of stirring in the dark to establish adsorption–desorption equilibrium, confirms the high starting concentration of the dye prior to photocatalytic irradiation. Upon exposure to natural solar light, the absorbance spectra demonstrate a clear and systematic decline in intensity, reflecting the time-dependent photocatalytic degradation of MB. After 13 min of sunlight exposure, the characteristic peak at 664 nm decreases noticeably, marking the onset of dye breakdown.

This decline continues with increasing irradiation time: by 25 min, the peak has further diminished, and by 70 min, a significant reduction is evident, with the absorption features becoming faint. At 90 min, the spectra show very low absorbance, indicating that the majority of MB molecules have been degraded. The subsequent spectra at 97 and 115 min are nearly flat, approaching the baseline and suggesting that the dye has been almost entirely removed from the solution. Finally, by 200 min, the spectrum is essentially a horizontal line near zero absorbance, confirming complete or near-complete degradation under the given experimental conditions. This sequential decrease in absorbance directly demonstrates the strong photocatalytic efficiency of the green-synthesized ZnO nanoparticles under solar irradiation. The progressive reduction of the characteristic MB peaks highlights the generation of reactive oxidative species on the ZnO surface, which attack the dye molecules and break down their chromophoric structure. This is well-established mechanism in photocatalysis [39]. The nearly zero absorbance values at extended irradiation times confirm that the photocatalytic process is highly effective, achieving substantial dye removal

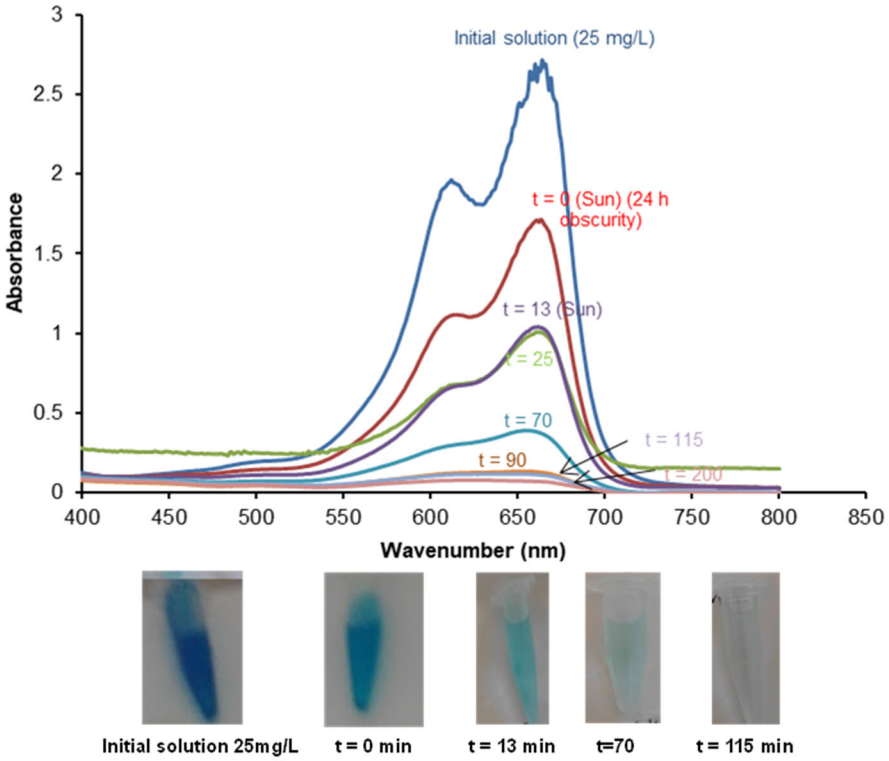

Fig 5. UV-vis absorption spectra and visual color change of MB during photocatalytic degradation by ZnO synthesized using olive wood ash extract under solar light

within a reasonable period. Overall, the UV–vis spectra provide compelling evidence that the synthesized ZnO nanoparticles function as an efficient solar-activated photocatalyst, capable of facilitating the complete photodegradation of MB in aqueous solution. The photocatalytic degradation of MB dye by the green-synthesized ZnO nanoparticles under natural solar light was visually confirmed by observing the progressive color change of the solution over time. As depicted in Fig. 5, the initial 25 mg/L MB solution exhibited a deep, characteristic blue hue. Upon exposure to solar irradiation, the solution color visibly lightened, transitioning to a pale blue by 13 min, and further diminishing to a faint greenish tint at 70 min. By 115 min, the solution became nearly colorless, providing compelling visual degradation of MB. Fig. 6 presents a comparative analysis of MB dye retention and subsequent photocatalytic degradation by green ZnO and that prepared by a conventional precipitation method. The experiment is clearly delineated into 2 critical phases: an initial adsorption phase conducted under obscurity and a subsequent photocatalytic degradation phase driven by natural solar light. This two-step process is crucial for distinguishing between dye adsorption and photocatalytic degradation [40]. During the initial adsorption phase, both the green-synthesized ZnO and the conventionally prepared ZnO demonstrate a consistent and comparable ability to retain MB dye from the solution. Both materials show a gradual increase in the percentage of MB retained over time when kept in the dark. This initial retention, reaching approximately 40% within the first 2 to 3 h, is solely attributable to the adsorption of MB molecules onto the surface of the ZnO nanoparticles. This phase is crucial for establishing a dark equilibrium, ensuring that any subsequent reduction in dye concentration during light exposure is a result of photocatalytic activity rather than mere surface adsorption. Following the adsorption equilibrium, the experiment transitions into the photocatalytic degradation phase, where the MB ZnO suspensions are exposed to natural sunlight. This phase, represented on the right side of the graph, reveals a significant divergence in the performance of the two ZnO materials. The green-synthesized ZnO exhibits superior photocatalytic efficiency, demonstrating a remarkably rapid and almost complete degradation of MB, which reaches nearly 99% degradation within 2 h of sunlight exposure under static conditions without stirring or agitation. This high efficiency underscores the effectiveness of the green synthesis approach in producing a robust photocatalyst, often attributed to the smaller particle size and higher surface area conferred by plant extracts [26]. In contrast, the conventional ZnO, while still demonstrating considerable photocatalytic

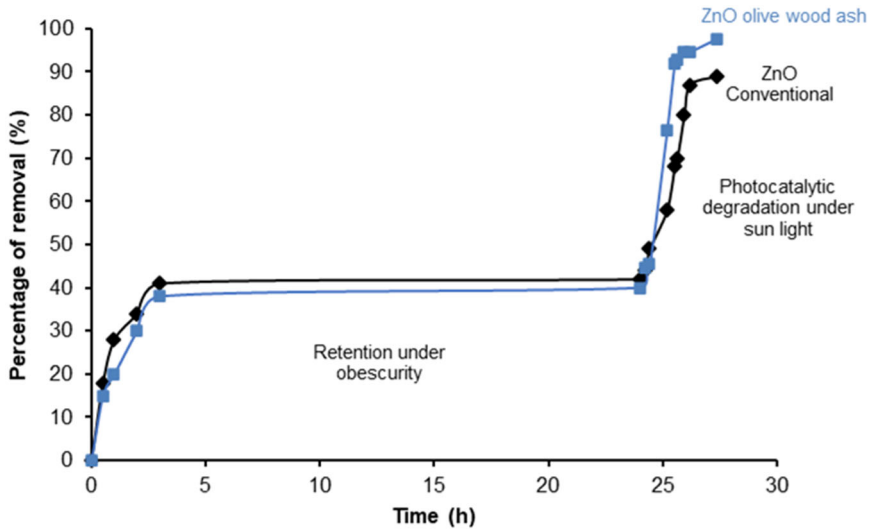

Fig 6. MB retention by adsorption under obscurity and photocatalytic removal under solar light using ZnO synthesized using olive wood ash extract and conventional ZnO

activity, shows a slightly lower degradation efficiency and a comparatively slower degradation rate. Within the same 2 h timeframe, the conventional ZnO achieves approximately 88% degradation. The less steep slope of its curve signifies that the MB molecules are degraded at a slower pace compared to the green synthesized counterpart materials. This difference in performance based on the synthesis method is a widely observed phenomenon [41].

Kinetic Study

The Langmuir–Hinshelwood (L–H) model was utilized to describe solid-catalyzed reactions, comprising four key stages: 1) adsorption of molecules onto the catalyst surface, 2) dissociation of the adsorbed molecules, 3) reaction of the dissociated species to form products, and 4) desorption of the resulting products from the surface. This model has been applied to the heterogeneous catalytic breakdown of organic pollutants in wastewater [42-44]. This model establishes a correlation between the degradation rate (r) and the concentration of the reactant in the aqueous phase at a specific time (C), using Eq. (5) [42-44];

$$r = -\frac{dC}{dt} = \frac{k_r K_{ad} C}{1 + K_{ad}} \quad (5)$$

where, k_r is the rate constant and K_{ad} is the adsorption equilibrium constant. When the adsorption is relatively weak and/or the reactant concentration is low, factor $K_{ad}C$ is negligible. As a result, Eq. (4) can be simplified to the pseudo-first order kinetics with an apparent first-order rate constant k_{app}, using Eq. (6) [43];

$$r = -\frac{dC}{dt} = k_{app} t \quad (6)$$

when, t = 0, C = C_0, and C_0 are the initial concentrations of MB after achieving adsorption–desorption equilibrium, integration of Eq. (5) can lead, using Eq. (7) [45];

$$\ln\left(\frac{C_0}{C_t}\right) = k_{app} t \quad (7)$$

where, C_0 is the initial concentration.

Fig. 7 illustrates the pseudo-first-order kinetics of MB photocatalytic degradation under solar irradiation, following the L–H model at an MB concentration of 25 mg/L. For chemically synthesized ZnO, the linear fit is y = 0.011x – 0.121 with R^2 = 0.994, giving an apparent rate constant (k_{app}) of 0.011/min. This corresponds to moderate degradation kinetics, achieving approximately 88% MB removal in 2 h, limited by its 3.37 eV bandgap and higher electron–hole recombination. In contrast, green-synthesized ZnO (using olive ash extract as precipitant) exhibits a linear fit of y = 0.015x – 0.187 with R^2 = 0.993, yielding k_{app} = 0.015/min—about 36% higher than the chemical ZnO. This enhanced rate enables ~99% MB removal within the same period, attributed to a narrower 2.8 eV bandgap. The high R^2 values (> 0.99) confirm excellent adherence to pseudo-first-order kinetics for both materials, validating the applicability of the L–H model. The superior k_{app} of green ZnO highlights its enhanced photocatalytic efficiency, making it a promising candidate for scalable wastewater treatment.

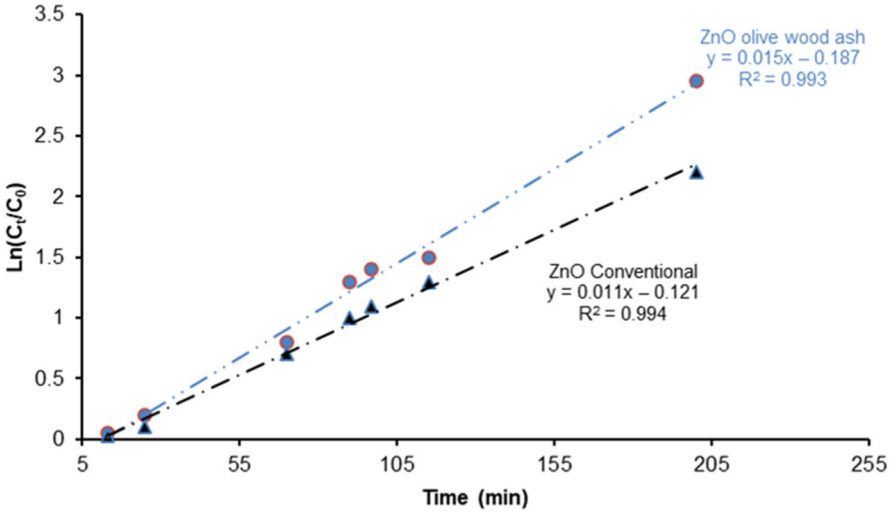

Fig 7. Kinetic analysis of photocatalytic MB removal using conventional and green ZnO synthesized

Table 1. Comparative table of kinetic of first-order rate constant k_{app} of some photocatalysts reported in the literature

Photocatalyst	Method of synthesis	Irradiation	k_{app} (/min)	Sources
TiO_2	Commercial TiO_2 'BIOCHEM ChemoPharma'	Solar	0.0060	[45]
ZnO	Commercial 'Aldrich'		0.0780	[45]
ZnO film	Doctor Blade method deposition	Visible LED	0.0020	[46]
ZnO:Ag 1%			0.0027	
ZnO:Ag 3%			0.0034	
ZnO:Ag 5%			0.0041	
TiO_2	Commercial 'Degussa'	Solar	0.0010	[47]
ZnO	Chemical precipitation (NaOH)		0.0015	[47]
ZnO/PEO-2			0.0021	
ZnO/PEO-6			0.0026	
ZnO/PEO-9			0.0024	
ZnO			0.0102	[42]
Al doped ZnO			0.0094	
Ce doped ZnO			0.0153	
ZnO	Conventional (Chemical precipitation by NaOH)		0.0110	This study
	Green (green precipitation by alkaline wood ash)		0.0150	

Table 1 compares k_{app} (1/min) for photocatalytic degradation using MB using various photocatalysts reported in the literature with this study's ZnO variants, conventional (k_{app} = 0.011/min) and green (k_{app} = 0.015/min) under solar irradiation. k_{app} ranges from 0.001 (commercial TiO_2, Degussa) to 0.078/min (commercial ZnO, Aldrich), reflecting diverse synthesis methods and materials. Visible LED entries (ZnO films/Ag-doped) show lower rates (0.002–0.0041/min.), highlighting limited visible-light efficacy. The current conventional ZnO (k_{app} = 0.011/min) exceeds most chemical/commercial solar catalysts (e.g., 0.001–0.0026/min for TiO_2, NaOH-ZnO/PEO composites) and aligns closely with undoped ZnO (0.0102/min), suggesting robust baseline performance without doping. The green ZnO (k_{app} = 0.015/min) outperforms all undoped solar entries, matching Ce-doped ZnO (0.0153/min) and surpassing Al-doped ZnO (0.0094/min), driven by its 2.8 eV bandgap (vs. 3.37 eV for the conventional method).

Limitations and Future Work

While this study serves as a robust proof-of-concept for a groundbreaking synthesis route, a comprehensive assessment requires further investigation. The following limitations will guide future research to elevate this foundational work: Material characterization: it is acknowledged that a full understanding of structural properties requires transmission electron microscopy (TEM) to complement SEM findings and provide detailed analysis of individual particle morphology, size distribution, and crystal lattice structure.

Environmental safety and toxicity: A comprehensive evaluation of the long-term environmental safety is crucial. Future work must include an in-depth analysis of potential heavy metal leaching and other toxic effects from the ash impurities into water. Reproducibility and Scalability: As the chemical composition of natural ash sources can vary, a full reproducibility analysis is required. Future work must establish a standardized synthesis protocol that accounts for these batch variations and includes a detailed economic analysis and life cycle assessment to confirm the cost benefits and viability of the method for large-scale industrial production.

Scope and Applicability: The scope of application will be expanded in future studies to include the degradation of anionic dyes (e.g. methyl orange) and complex pollutant matrices found in real industrial wastewater.

■ CONCLUSION

This study successfully demonstrates a sustainable and eco-friendly route for synthesizing green ZnO nanoparticles by utilizing OWCA extract as a natural, highly alkaline precipitating agent. Comprehensive characterization confirmed the formation of a highly crystalline hexagonal structure and revealed a crucial optical modification: the green synthesized ZnO exhibited a significantly narrowed direct band gap of 2.8 eV, a notable decrease from the 3.3 eV found in conventional ZnO. This narrowing, attributed to intrinsic defects and potential trace doping, substantially enhanced the material's light absorption capabilities. The superior performance was unequivocally demonstrated in the degradation of MB under natural solar light, where the green ZnO achieved nearly 99% degradation within just 2 h. By valorizing agricultural waste (OWCA) into a high-value, solar-activated photocatalyst, this research strongly contributes to circular economy principles, offering a promising and sustainable alternative for advanced wastewater treatment and solar energy applications.

■ ACKNOWLEDGMENTS

The experimental work was carried out at the Laboratory of Textile Engineering (LGTEx) in Ksar Hellal, Tunisia. The authors are grateful to the LGTEx team for their support and for providing the necessary facilities to conduct the experiments. The subsequent characterization of the samples was performed at the Borj Cedria Science and Technology Park in Tunis, which provided a key role in the analysis of the data. The authors also acknowledge no financial support from grants, institutions, or other funding bodies that made this research possible.

■ CONFLICT OF INTEREST

The authors declare that there are no conflicts of interest regarding the publication of this manuscript.

■ AUTHOR CONTRIBUTIONS

Data curation: Sana Fridjine; Formal analysis: Nedra Abbes, Thouraya Barhoumi and Nejib Sejri; Funding acquisition: Jun Xu; Investigation: Thouraya Barhoumi; Methodology: Nedra Abbes and Sana Fridjine; Resources: Imene Bekri-Abess; Supervision: Boubaker Jaouachi and Imene Bekri-Abess; Validation: Boubaker Jaouachi and Imene Bekri-Abess; Writing – original draft: Nedra Abbes. All authors have read and agreed to the published version of the manuscript.

■ REFERENCES

[1] Tissera, N.D., Wijesena, R.N., Sandaruwan, C.S., de Silva, R.M., de Alwis, A., and de Silva, K.M.N., 2018, Photocatalytic activity of ZnO nanoparticle encapsulated poly(acrylonitrile) nanofibers, *Mater. Chem. Phys.*, 204, 195–206.

[2] Abdelmigid, H.M., Hussien, N.A., Alyamani, A.A., Morsi, M.M., AlSufyani, N.M., and Kadi, H.A., 2022, Green synthesis of zinc oxide nanoparticles using pomegranate fruit peel and solid coffee grounds vs. chemical method of synthesis, with their biocompatibility and antibacterial properties investigation, *Molecules*, 27 (4), 1236.

[3] Hu, S.H., Chen, Y.C., Hwang, C.C., Peng, C.H., and Gong, D.C., 2010, Development of a wet chemical method for the synthesis of arrayed ZnO nanorods, *J. Alloys Compd.*, 500 (2), L17–L21.

[4] Kadinskaya, S.A., Kondratev, V.M., Kindyushov, I.K., Koval, O.Y., Yakubovsky, D.I., Kusnetsov, A., Lihachev, A.I., Nashchekin, A.V., Akopyan, I.K., Serov, A.Y., Labzovskaya, M.E., Mikushev, S.V., Novikov, B.V., Shtrom, I.V., and Bolshakov, A.D., 2023, Deep-level emission tailoring in ZnO nanostructures grown via hydrothermal synthesis, *Nanomaterials*, 13 (1), 58.

[5] Al-Dhabi, N.A., and Valan Arasu, M., 2018, Environmentally-friendly green approach for the production of zinc oxide nanoparticles and their anti-fungal, ovicidal, and larvicidal properties, *Nanomaterials*, 8 (7), 500.

[6] Fakhirah, D., Magfira, T.A., Hutama, A.S., Septama, A.W., Maryani, F., and Krismastuti, F.S.H., 2024, Synthesis, characterization, and antibacterial activity of plant-derived zinc oxide nanostructure using *Lavandula angustifolia* and *Phyllanthus niruri* extracts, *Indones. J. Chem.*, 24 (3), 865–875.

[7] Khalafi, T., Buazar, F., and Ghanemi, K., 2019, Phycosynthesis and enhanced photocatalytic activity of zinc oxide nanoparticles toward organosulfur pollutants, *Sci. Rep.*, 9 (1), 6866.

[8] Kalaba, M.H., Moghannem, S.A., El-Hawary, A.S., Radwan, A.A., Sharaf, M.H., and Shaban, A.S., 2021, Green synthesized ZnO nanoparticles mediated by *Streptomyces plicatus*: Characterizations, antimicrobial and nematicidal activities and cytogenetic effects, *Plants*, 10 (9), 1760.

[9] Ahmad, W., and Kalra, D., 2020, Green synthesis, characterization and anti-microbial activities of ZnO nanoparticles using *Euphorbia hirta* leaf extract, *J. King Saud Univ., Sci.*, 32 (4), 2358–2364.

[10] Trevisan, J., and dos Santos, A.C.P., 2024, "Ash Soap Preserving the Environment" in *Multidisciplinary Research and Practice*, Seven Editora, São José dos Pinhais, Paraná, Brazil, 662–668.

[11] Nogales, R., Delgado, G., Quirantes, M., Romero, M., Romero, E., and Molina-Alcaide, E., 2011, "Characterization of Olive Waste Ashes as Fertilizers" in *Recycling of Biomass Ashes*, Eds. Insam, H., and Knapp, B.A., Springer, Berlin, Germany, 57–68.

[12] Nasr, M., Balme, S., Eid, C., Habchi, R., Miele, P., and Bechelany, M., 2017, Enhanced visible-light photocatalytic performance of electrospun rGO/TiO_2 composite nanofibers, *J. Phys. Chem. C*, 121 (1), 261–269.

[13] Maatoq, S.L., and Ali, I.H., 2025, Green fabrication of silica with zinc oxide as nanocomposite for adsorption of methylene blue dye from aqueous solution, *Indones. J. Chem.*, 25 (5), 1451–1461.

[14] Ong, C.B., Ng, L.Y., and Mohammad, A.W., 2018, A review of ZnO nanoparticles as solar photocatalysts: Synthesis, mechanisms and applications, *Renewable Sustainable Energy Rev.*, 81, 536–551.

[15] Palma De Oliveira, D., Zanoni, M.V., Chequer, F., Oliveira, G., Cardoso, J., and Ferraz, E., 2013, "Textile Dyes: Dyeing Process and Environmental Impact" in *Eco-Friendly Textile Dyeing and Finishing*, IntechOpen, London, UK.

[16] Bedoui, K., Bekri-Abbes, I., and Srasra, E., 2008, Removal of cadmium (II) from aqueous solution using pure smectite and Lewatite S 100: The effect of time and metal concentration, *Desalination*, 223 (1), 269–273.

[17] Happy, A., Soumya, M., Venkat Kumar, S., Rajeshkumar, S., Sheba, R.D., Lakshmi, T., and Deepak Nallaswamy, V., 2019, Phyto-assisted synthesis of zinc oxide nanoparticles using *Cassia alata* and its antibacterial activity against *Escherichia coli*, *Biochem. Biophys. Rep.*, 17, 208–211.

[18] Ramesh, M., Anbuvannan, M., and Viruthagiri, G., 2015, Green synthesis of ZnO nanoparticles using *Solanum nigrum* leaf extract and their antibacterial activity, *Spectrochim. Acta, Part A*, 136, 864–870.

[19] Kadri, Y., Srasra, E., Bekri-Abbes, I., and Herrasti, P., 2021, Facile and eco-friendly synthesis of polyaniline/ZnO composites for corrosion protection of AA-2024 aluminium alloy, *J. Electroanal. Chem.*, 893, 115335.

[20] Hanna, A.L., Hamouda, H.M., Goda, H.A., Sadik, M.W., Moghanm, F.S., Ghoneim, A.M., Alenezi, M.A., Alnomasy, S.F., Alam, P., and Elsayed, T.R., 2022, Biosynthesis and characterization of silver nanoparticles produced by *Phormidium ambiguum* and *Desertifilum tharense* cyanobacteria, *Bioinorg. Chem. Appl.*, 2022 (1), 9072508.

[21] Fazlzadeh, M., Khosravi, R., and Zarei, A., 2017, Green synthesis of zinc oxide nanoparticles using *Peganum harmala* seed extract, and loaded on *Peganum harmala* seed powdered activated carbon as new adsorbent for removal of Cr(VI) from aqueous solution, *Ecol. Eng.*, 103, 180–190.

[22] Frost, R.L., and Dickfos, M.J., 2007, Raman spectroscopy of halogen-containing carbonates, *J. Raman Spectrosc.*, 38 (11), 1516–1522.

[23] Abdelbaky, A., Abd El-Mageed, T., Babalghith, A., Selim, S., and Mohamed, A., 2022, Green synthesis and characterization of ZnO nanoparticles using *Pelargonium odoratissimum* (L.) aqueous leaf extract and their antioxidant, antibacterial and anti-inflammatory activities, *Antioxidants*, 11 (8), 1444.

[24] Yanuhar, U., Suryanto, H., Amin, M., Binoj, J.S., and Casuarina, I., 2024, Green synthesis of nano-

copper oxide using *Sargassum* sp. functionalized in cellulose acetate membrane for dye adsorption, *Global J. Environ. Sci. Manage.*, 10 (4), 1933–1950.

[25] Okaiyeto, K., Gigliobianco, M.R., and Di Martino, P., 2024, Biogenic zinc oxide nanoparticles as a promising antibacterial agent: Synthesis and characterization, *Int. J. Mol. Sci.*, 25 (17), 9500.

[26] Mahajan, M., Kumar, S., Gaur, J., Kaushal, S., Dalal, J., Singh, G., Misra, M., and Ahlawat, D.S., 2025, Green synthesis of ZnO nanoparticles using *Justicia adhatoda* for photocatalytic degradation of malachite green and reduction of 4-nitrophenol, *RSC Adv.*, 15 (4), 2958–2980.

[27] Pascariu, P., Gherasim, C., and Airinei, A., 2023, Metal oxide nanostructures (MONs) as photocatalysts for ciprofloxacin degradation, *Int. J. Mol. Sci.*, 24 (11), 9564.

[28] Silveira, M.L.D.C., da Silva, N.R., Padovini, D.S.S., Kinoshita, A., Pontes, F.M.L., and Magdalena, A.G., 2022, Synthesis, characterization, and photocatalytic activity of ZnO nanostructures, *Res. Soc. Dev.*, 11 (2), e3811225373.

[29] Jayachandraiah, C., Siva Kumar, K., Krishnaiah, G., and Madhusudhana Rao, N., 2015, Influence of Dy dopant on structural and photoluminescence of Dy-doped ZnO nanoparticles, *J. Alloys Compd.*, 623, 248–254.

[30] Franco Jr, A., and Pessoni, H.V.S., 2017, Effect of Gd doping on the structural, optical band-gap, dielectric and magnetic properties of ZnO nanoparticles, *Phys. B*, 506, 145–151.

[31] Joshi, R., 2018, Facile photochemical synthesis of ZnO nanoparticles in aqueous solution without capping agents, *Materialia*, 2, 104–110.

[32] Ansari, S.A., Khan, M.M., Kalathil, S., Nisar, A., Lee, J., and Cho, M.H., 2013, Oxygen vacancy induced band gap narrowing of ZnO nanostructure by electrochemically active biofilm, *Nanoscale*, 5 (19), 9238–9246.

[33] Kumar Jangir, L., Kumari, Y., Kumar, A., Kumar, M., and Awasthi, K., 2017, Investigation of luminescence and structural properties of ZnO nanoparticles, synthesized with different precursors, *Mater. Chem. Front.*, 1 (7), 1413–1421.

[34] Coates, J., 2000, "Interpretation of Infrared Spectra, A Practical Approach" in *Encyclopedia of Analytical Chemistry*, Eds. Meyers, R.A., John Wiley & Sons Ltd., Chichester, UK, 10815–10837.

[35] Movasaghi, Z., Rehman, S., and Ur Rehman, I., 2008, Fourier transform infrared (FTIR) spectroscopy of biological tissues, *Appl. Spectrosc. Rev.*, 43 (2), 134–179.

[36] Ezealisiji, K.M., Siwe-Noundou, X., Maduelosi, B., Nwachukwu, N., and Krause, R.W.M., 2019, Green synthesis of zinc oxide nanoparticles using *solanum torvum* (L.) leaf extract and evaluation of the toxicological profile of the ZnO nanoparticles–hydrogel composite in Wistar albino rats, *Int. Nano Lett.*, 9 (2), 99–107.

[37] Judith Vijaya, J., Jayaprakash, N., Kombaiah, K., Kaviyarasu, K., John Kennedy, L., Jothi Ramalingam, R., Al-Lohedan, H.A., Mansoor-Ali, V.M., and Maaza, M., 2017, Bioreduction potentials of dried root of *Zingiber officinale* for a simple green synthesis of silver nanoparticles: Antibacterial studies, *J. Photochem. Photobiol., B*, 177, 62–68.

[38] Kayaci, F., Vempati, S., Donmez, I., Biyikli, N., and Uyar, T., 2014, Role of zinc interstitials and oxygen vacancies of ZnO in photocatalysis: A bottom-up approach to control defect density, *Nanoscale*, 6 (17), 10224–10234.

[39] Saad Algarni, T., Abduh, N.A.Y., Al Kahtani, A., and Aouissi, A., 2022, Photocatalytic degradation of some dyes under solar light irradiation using ZnO nanoparticles synthesized from *Rosmarinus officinalis* extract, *Green Chem. Lett. Rev.*, 15 (2), 460–473.

[40] Vallejo, W., Diaz-Uribe, C.E., and Duran, F., 2023, Kinetic and thermodynamic study of methylene blue adsorption on TiO_2 and ZnO thin films, *Materials*, 16 (12), 4434.

[41] Krobthong, S., Rungsawang, T., and Wongrerkdee, S., 2023, Comparison of ZnO nanoparticles prepared by precipitation and combustion for UV

and sunlight-driven photocatalytic degradation of methylene blue, *Toxics*, 11 (3), 266.

[42] Ameen, S., Fatima, R., Kadhem, A.A., Abbas, T., Khan, M.A., Abbas, A., Hussain, I., Bano, N., Faraji Rad, Z., and Bilal, A.S.S., 2025, Enhanced photocatalytic degradation of methylene blue using aluminum and cerium co-doped ZnO nanocomposite, *Int. J. Environ. Sci. Technol.*, 22 (16), 16549–16558.

[43] Petukhov, A.V., 1997, Effect of molecular mobility on kinetics of an electrochemical Langmuir-Hinshelwood reaction, *Chem. Phys. Lett.*, 277 (5-6), 539–544.

[44] Tran, H.D., Nguyen, D.Q., Do, P.T., and Tran, U.N.P., 2023, Kinetics of photocatalytic degradation of organic compounds: A mini-review and new approach, *RSC Adv.*, 13 (25), 16915–16925.

[45] Chekir, N., Benhabiles, O., Tassalit, D., Laoufi, N.A., and Bentahar, F., 2016, Photocatalytic degradation of methylene blue in aqueous suspensions using TiO_2 and ZnO, *Desalin. Water Treat.*, 57 (13), 6141–6147.

[46] Vallejo, W., Cantillo, A., and Díaz-Uribe, C., 2020, Methylene blue photodegradation under visible irradiation on Ag-doped ZnO thin films, *Int. J. Photoenergy*, 2020 (1), 1627498.

[47] Marković, S., Rajić, V., Stanković, A., Veselinović, L., Belošević-Čavor, J., Batalović, K., Abazović, N., Škapin, S.D., and Uskoković, D., 2016, Effect of PEO molecular weight on sunlight induced photocatalytic activity of ZnO/PEO composites, *Sol. Energy*, 127, 124–135.